

# Fast Geometric Sound Propagation with Finite-Edge Diffraction

LAKULISH ANTANI, ANISH CHANDAK, MICAH TAYLOR and DINESH MANOCHA

University of North Carolina at Chapel Hill

TR10-011

We present a fast algorithm to accelerate geometric sound propagation in complex 3D scenes. Our approach computes propagation paths from each source to the listener by taking into account specular reflections and higher-order edge diffractions around finite edges in the scene. We use the well known Biot-Tolstoy-Medwin (BTM) diffraction model along with efficient algorithms for region-based visibility to cull away primitives and significantly reduce the number of edge pairs that need to be processed. The performance of region-based visibility computation is improved by using a fast occluder selection algorithm that can combine small, connected triangles to form large occluders and perform conservative computations at object-space precision. We show that our approach is able to reduce the number of visible primitives considered for sound propagation by a factor of 2 to 4 for second order edge diffraction as compared to prior propagation algorithms. We demonstrate and analyze its performance on multiple benchmarks. To the best of our knowledge, this is the first algorithm that uses object-space visibility algorithms to accelerate finite-edge diffraction computation for geometric sound propagation.

Categories and Subject Descriptors: I.3.7 [Computer Graphics]: Three-Dimensional Graphics and Realism—*Virtual reality, Visible line/surface determination*; I.3.8 [Computer Graphics]: Applications

General Terms: Performance

Additional Key Words and Phrases: visibility, object-space, from-region, sound propagation, diffraction

## 1. INTRODUCTION

Sound rendering or auditory displays can augment graphical rendering and provide the user with an enhanced spatial sense of presence. Some of the driving applications of sound rendering include acoustic design of architectural models or outdoor scenes, walkthroughs of large CAD models with sounds of machine parts or moving people, urban scenes with traffic, training systems, computer games, etc. A key component in these applications is accurate

computation of sound propagation paths, which takes into account the knowledge of sound sources, listener locations, the 3D model of the environment, and material absorption and scattering properties.

There is extensive literature on simulating the propagation of sound, including reflections and diffraction. The propagation of sound in a medium is governed by the *acoustic wave equation*, a second-order partial differential equation [Svensson and Kristiansen 2002]. However, numerical methods that directly solve the acoustic wave equation can take tens of minutes even for simple rooms. Moreover, for numerical methods, the computation time grows as a fourth power of the maximum frequency simulated, and is proportional to the volume of the enclosed space. Hence they can only be used for small rooms and for low frequencies. On the other hand, fast sound propagation methods are based on geometric techniques such as ray tracing or volumetric tracing. These methods work well in terms of handling specular reflections, and can take advantage of recent advances in real-time ray tracing methods and multi-core processors. However, current geometric propagation methods are either not fast enough for interactive applications or may not compute all propagation paths accurately. As a result, interactive applications such as computer games tend to use statically designed environment reverberation filters. Some games use ray tracing to estimate the size of a room and use this information to set parameters for a reverberation filter. Games also use precomputed visibility to determine if a source is out of line of sight from the listener. This is usually performed at a coarse level, i.e., visibility is determined at a room-to-room level of detail using cell-and-portal visibility [Luebke and Georges 1995] or ray shooting. If the source is not visible, a low-pass filter is usually applied to approximate diffraction effects. However the direction is the direct line from source to listener, which leads to very unnatural sound which seems to emanate from solid walls.

In this paper, we primarily focus on simulating edge diffraction for geometric sound propagation. Diffraction is an important effect that causes sound to scatter when encountering the finite boundaries of objects, resulting in audio energy being propagated to positions that are out of line-of-sight from the source. Diffraction also affects the sound field at positions that are visible to the source. For example, for a small specular reflector, edge diffraction causes a high-pass filter effect when the listener is visible to the source; capturing these diffraction contributions is important for an accurate simulation. In acoustic simulation, diffraction effects are primarily modeled at the edges of the objects in the scene. The computation of diffraction effects can convey important audio cues from sources that are not visible to the listener, and allow more listener positions to receive contributions from the sound source. Most importantly, when the listener or the source is moving, specular reflections and direct contributions abruptly appear and disappear as the source or listener moves across visibility boundaries. Therefore, it is necessary to simulate diffraction accurately in order to obtain a more realistic and smooth transition.

---

Authors' email: (lakulish, achandak, taylormt, dm)@cs.unc.edu.

Permission to make digital or hard copies of part or all of this work for personal or classroom use is granted without fee provided that copies are not made or distributed for profit or commercial advantage and that copies show this notice on the first page or initial screen of a display along with the full citation. Copyrights for components of this work owned by others than ACM must be honored. Abstracting with credit is permitted. To copy otherwise, to republish, to post on servers, to redistribute to lists, or to use any component of this work in other works requires prior specific permission and/or a fee. Permissions may be requested from Publications Dept., ACM, Inc., 2 Penn Plaza, Suite 701, New York, NY 10121-0701 USA, fax +1 (212) 869-0481, or permissions@acm.org.

© ACM 0730-0301/10-ART \$10.00

DOI

<http://doi.acm.org/>

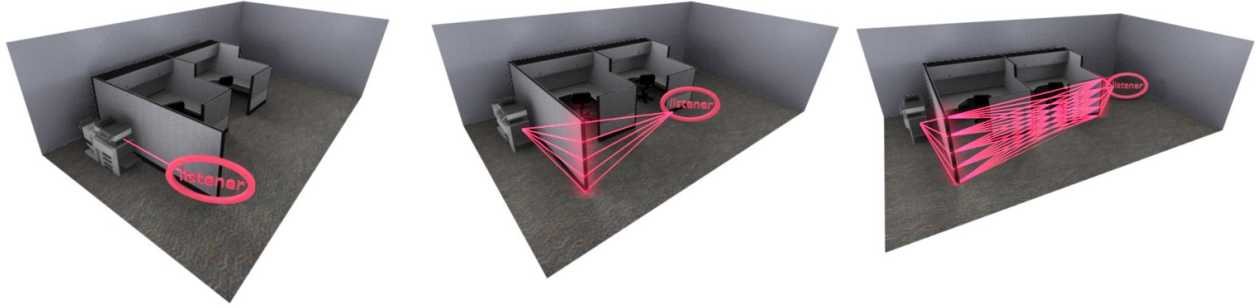


Fig. 1. Propagation paths for the sound of an office printer as it diffracts around cubicle edges and reaches the listener. Left to right: (a) direct sound (b) first-order diffraction (c) second-order diffraction. Our algorithm can accelerate second-order diffraction on such benchmarks by a factor of 2–4.

In the context of geometric propagation, two main approaches exist for modeling edge diffraction: the Uniform Theory of Diffraction (UTD) [Kouyoumjian and Pathak 1974] and the Biot-Tolstoy-Medwin (BTM) [Biot and Tolstoy 1957; Medwin et al. 1982] model. UTD models diffraction around an infinite edge in terms of a single virtual point source on the edge. While this makes it fast enough to be useful in interactive applications [Tsingos et al. 2001; Taylor et al. 2009], it is an approximate method and may only work well for models with very large edges in outdoor scenes. On the other hand, BTM models diffraction around *finite* edges in terms of many virtual point sources located along the edge (see Figure 1). Although this makes the resulting approach more computationally intensive than UTD, it has been shown to be more accurate than UTD at low frequencies, where diffraction effects play an important role [Svensson et al. 1999].

**Main Results** We present an algorithm for fast geometric sound propagation based on the BTM model in static scenes with moving sources and listeners. Our approach is based on the fact that a BTM-based propagation algorithm requires the capability to determine which other diffracting edges are visible from a given diffracting edge. This reduces to a *from-region visibility* problem, and we use a conservative from-region visibility algorithm which can compute the set of visible triangles and edges at object-space precision in a conservative manner. Most of the prior work on from-region visibility has been restricted to accelerating real-time visual rendering or global illumination for image synthesis. We are not aware of any application of from-region algorithms that are used to accelerate finite edge diffraction.

In order to accurately compute the propagation paths, it is important to perform the visibility computations at object-space precision and use conservative algorithms [Lehnert 1993; Begault 1994; Chandak et al. 2009]. We also present a novel occluder selection algorithm that can improve the performance of from-region visibility computation on large, complex models and perform accurate computation.

The main contributions of this paper are as follows:

- Accelerated higher-order BTM diffraction.** We present a fast algorithm to accurately compute the first few orders of diffraction using the BTM model. We use object-space conservative from-region visibility to significantly reduce the number of edge

pairs that need to be considered as compared to the state-of-the-art for second order diffraction. We demonstrate that for scenes that are used in room acoustics, our approach can use visibility algorithms to improve the performance of BTM edge diffraction algorithms by a factor of 2 to 4.

- Effective occluder selection for region-based visibility.** We present a fast algorithm for occluder selection that can compute occluders in all directions around a given convex region. Our algorithm can combine connected sets of small primitives into large occluders and can be more effective in terms of culling efficiency. The final set of visible primitives can then be computed using a state-of-the-art occlusion culling technique. We demonstrate that our occluder selection technique is able to quickly generate occluders consisting of 2-6 triangles each on the average in complex scenes in a few seconds per visibility query on a single core.

We show that our approach is able to reduce the amount of visible geometry considered by sound propagation algorithms by a factor of 2 to 4 for second-order edge diffraction. This allows us to obtain a speedup factor of 2 to 4 when simulating second-order edge diffraction using the BTM model on our benchmark scenes. The resulting conservative from-region visibility algorithm can also be applied to complex models with hundreds of thousands of triangles.

**Outline** The rest of this paper is organized as follows: Section 2 describes background material and related work. Section 3 describes our approach of using visibility computations to accelerate BTM diffraction computations. Section 4 describes our novel occluder selection technique and its use to improve the performance of from-region visibility algorithms. Section 5 describes our implementation and presents experimental results.

## 2. BACKGROUND

In this section, we give a brief overview of background material on sound propagation algorithms, region-based visibility computation and image-source methods for geometric sound propagation.

## 2.1 Sound Propagation

The acoustic properties of a scene are described using the *impulse response* (IR). The IR is computed at the listener's position, and represents the pressure signal arriving at the listener for a unit impulse signal emitted by the isotropic point source. Sound propagation in rooms can be modeled as a linear phenomenon [Kuttruff 1991], which implies that given an arbitrary anechoic sound signal emitted by the source, the signal received by the listener (taking into account propagation effects) can be obtained by convolving the anechoic signal with the impulse response.

The propagation of sound in a medium is governed by the *acoustic wave equation*, a second-order partial differential equation [Svensson and Kristiansen 2002]. Several methods exist that directly solve the wave equation using numerical methods [Ciskowski and Brebbia 1991; Lehtinen 2003] and accurately model sound propagation in a scene. However, despite recent advances [Raghuvanshi et al. 2008], these methods can take tens of minutes to compute the impulse responses and can be too slow for real-time applications.

Most sound propagation techniques used in practical applications model the acoustic effects of an environment using linearly propagating rays. These *geometric acoustics* (GA) techniques are not as accurate as numerical methods in terms of solving the wave equation, and cannot easily model all kinds of propagation effects, but they allow simulation of early reflections at real-time rates.

Specular reflections are easy to model using GA methods. The most common methods include the image source method [Allen and Berkley 1979; Funkhouser et al. 1998; Schröder and Lentz 2006; Laine et al. 2009], ray tracing [Krokstad et al. 1968; Vorländer 1989] and approximate volume tracing [Lauterbach et al. 2007; Chandak et al. 2008]. Of these methods, the image source method is the most accurate, since it is guaranteed to not miss any specular propagation paths between the source and the listener. GA methods are also used for modeling diffuse reflections. The two main techniques of doing so are based on path tracing [Dalenbäck 1996; Kapralos et al. 2004] and radiosity [Siltanen et al. 2007; Siltanen et al. 2009].

Diffraction is relatively difficult to model using GA techniques (as compared to specular reflections), because it involves sound waves bending around objects. The two commonly used geometric models of diffraction are the Uniform Theory of Diffraction (UTD) [Kouyoumjian and Pathak 1974] and the Biot-Tolstoy-Medwin (BTM) model [Svensson et al. 1999]. The UTD model assumes infinite diffracting edges, an assumption which may not be applicable in real-world scenes (e.g., indoor scenes). However, UTD has been used successfully in interactive applications [Tsingos et al. 2001; Antonacci et al. 2004; Taylor et al. 2009]. BTM, on the other hand, deals with finite diffracting edges, and therefore is more accurate than UTD [Svensson et al. 1999]; however it is much more complicated and has only recently been used – with several approximations – in interactive applications [Schröder and Pohl 2009].

## 2.2 Image Source Method for Geometric Propagation

Given a point source  $S$  and a listener  $L$ , it is easy to check if a direct path exists from  $S$  to  $L$ . This is a ray shooting problem. The basic idea behind the image source method is as follows. For a specular reflector (in our case, a triangle)  $T$ , a specular path  $S \rightarrow T \rightarrow L$  exists if and only if a direct path exists from the *image* of  $S$

formed by  $T$ , to  $L$ , and this direct path also passes through  $T$ . In the absence of any visibility information, image sources need to be computed about *every* triangle in the scene. This process can be applied recursively to check for higher order specular paths from  $S$  to  $L$ , but the complexity can increase exponentially as a function of the number of reflections.

For a given source position, this process can be accelerated [Laine et al. 2009] as follows. Note that first-order image sources only need to be computed about triangles visible to  $S$ . For a first-order image source  $S_1$ , second-order image sources only need to be computed for the triangles that are visible to  $S_1$  through  $T$ , and so on for higher order image sources. It is also possible to integrate geometric models for edge diffraction into the image source framework [Pulkki et al. 2002]. In Section 3 we describe our method that uses from-point and from-region visibility algorithms to accelerate the GA algorithms which integrate edge diffraction effects into the image source method.

## 2.3 From-Region Visibility

Visibility computation is one of the classic problems studied extensively due to its importance in many fields such as computer graphics, computational geometry, and robotics. The problem of finding surfaces visible from a given *region*, such as a triangle, edge, or bounding box (i.e., the from-region visibility problem) is well-studied in the literature. We present a brief overview of prior work in this domain; for further details we refer the reader to detailed surveys of the field [Cohen-Or et al. 2003; Bittner and Wonka 2003]. Exact solutions can be computed using techniques such as aspect graphs [Gigus et al. 1991], visibility complex [Durand et al. 1996; Durand et al. 1997] or by computing unobstructed rays by performing CSG operations in a dual line space [Nirenstein et al. 2002]. These methods have high complexity –  $O(n^3)$  for aspect graphs and  $O(n^4)$  for the visibility complex, where  $n$  is the number of scene primitives – and are too slow to be of practical use on complex models.

Many methods exist which compute approximate visibility by essentially sampling the space of rays originating in the query region. These methods are fast enough to be practically useful on large and complex models [Wonka et al. 2006; Bittner et al. 2009], but have one important limitation: they compute a *subset* of the exact solution (i.e., approximate visibility), and therefore, are limited to sampling-based applications such as interactive graphical rendering, and may not provide sufficient accuracy for sound rendering. This is because the image source method requires us to find all possible propagation paths (see Section 2.2), which in turn requires the visibility algorithm to not miss any visible geometry. For a sampling-based algorithm in complex scenes, this can require a prohibitively high sampling frequency in order to guarantee that all visible geometry is returned in the output of the algorithm.

The other class of applicable algorithms is *conservative* visibility algorithms. These algorithms can efficiently compute a *superset* of the exact solution. Some conservative algorithms operate in dual ray space by finding *stabbing lines* [Teller and Séquin 1991] and dividing the scene into *cells* separated by *portals* [Teller 1992; Luebke and Georges 1995]. Other algorithms operate in primal space by performing *occlusion culling* with respect to *shadow frusta* [Durand et al. 2000; Chhugani et al. 2005].

Extended projections [Durand et al. 2000] use a conservative rasterization process along with depth comparisons to sweep an image

plane outward from the the view-region. Culling occurs by projecting occluders onto the image plane and then comparing the occluder depths to the depths of occludee projections. The algorithm requires convex 3D occluders or planar non-convex occluders.

One conservative algorithm uses a volumetric representation of the occluders [Schauffer et al. 2000]. This algorithm subdivides the environment using an octree into cells that are inside, outside, or intersecting occluders. A front-to-back traversal from the view-region computes umbrae of “inside” cells. The cells inside the umbrae are blocked. Occluder fusion is captured by enlarging occluders to encompass neighboring inside cells and previously blocked cells. The major limitation of this algorithm is that it only applies to environments that have closed or volumetric occluders.

Several algorithms are based on the concept of occluder shrinking [Wonka et al. 2000; Chhugani et al. 2005]. Occluder shrinking involves using a from-point projection with occluders that have been eroded to preserve conservativeness. Previous occluder shrinking algorithms were targeted at 2.5D urban environments. Chhugani et al. [2005] presented an algorithm for complex 3D environments and combined it with level-of-detail algorithms for interactive display.

Another approach [Leyvand et al. 2003] uses a factorization of the space of rays exiting a region along with a front-to-back traversal of the surrounding environment to perform culling. Their approach is amenable to a GPU implementation but assumes an axis along which there are significantly fewer visibility events.

Several algorithms compute conservative approximations of occluders or fused occluders [Law and Tan 1999; Koltun and Cohen-Or 2000]. Law and Tan [1999] provide an algorithm for computing levels-of-detail of closed 3D polyhedral objects that preserve occlusion. Koltun et al. [2000] provide an algorithm for replacing a disjoint set of 2D or 2.5D occluders by a virtual occluder with a conservative approximation of their fused umbra.

## 2.4 From-Point Visibility

Extensive work has been done to compute from-point visibility with object-space precision [Ghali 2001]. Exact from-point approaches based on Plücker coordinates [Nirenstein 2003] and beam tracing have been proposed [Heckbert and Hanrahan 1984] but they are compute intensive. The recent beam tracing approach presented by Overbeck et al. [2007] is efficient and has been applied for soft shadows. Conservative approaches for from-point visibility have been developed [Bittner et al. 1998; Coorg and Teller 1997; Hudson et al. 1997; Luebke and Georges 1995; Akenine-Möller and Aila 2005] but are limited to architectural scenes, 2.5D scenes, or scenes with large occluders. Chandak et al. [2009] proposed a from-point visibility algorithm for general 3D scenes which is significantly faster and computes visible sets within 10–25% of exact approaches [Overbeck et al. 2007].

## 3. SOUND PROPAGATION

Our geometric sound propagation algorithm is based on the image source method [Allen and Berkley 1979; Schröder and Lentz 2006]. As originally formulated, this technique can simulate specular reflections only. However, it is possible to extend this method to handle edge diffraction effects as well [Chambers and Berthelot 1994; Torres et al. 2001; Pulkki et al. 2002; Calamia et al. 2005]. In this

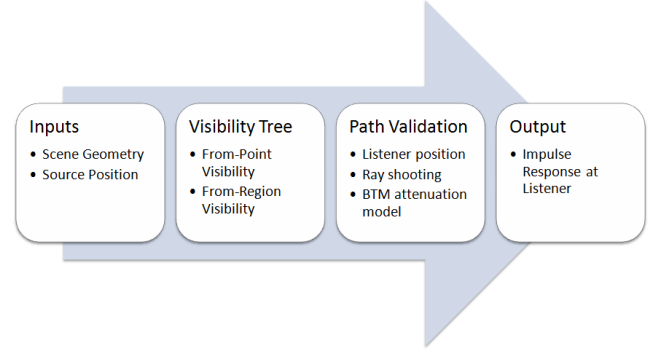


Fig. 2. Overview of our sound propagation algorithm. Using the scene geometry and source position as the input, we first construct a visibility tree that represents the potential propagation paths. Next, we use the listener position to find valid propagation paths using the visibility tree. Finally, we use the valid paths and the BTM model to compute the impulse response at the listener.

section, we present our efficient algorithm to perform diffraction using region-based visibility computations to accelerate the computations. Figure 2 gives an overview of our technique.

Broadly, our approach uses the fact that second-order edge diffraction need only be computed for edge pairs that are mutually visible. Therefore, our approach consists of two main steps. First, we use from-region visibility to determine which edges are visible from each of the diffracting edges in the scene. In the second step, we compute the diffraction contributions to the IR at the listener for each mutually visible edge pair. Algorithms 1–3 show the pseudocode of this approach. The pseudocode clearly shows the crucial role of visibility in the image source method.

---

### Algorithm 1 *ComputeImpulseResponse*( $S, L$ )

---

```

{  $S$  is the source position,  $L$  is the listener position }
depth  $\leftarrow 0$ 
VT  $\leftarrow \phi$ 
add node for  $S$  as root node in VT
VT  $\leftarrow \text{AddNodes}(\text{VT}, S, \text{depth})$ 
IR  $\leftarrow$  empty impulse response
node  $\leftarrow$  root node of VT
IR  $\leftarrow \text{IR} + \text{ValidatePath}(\text{node}, L, \text{IR})$ 
return IR
  
```

---

## 3.1 Edge Diffraction and Image Sources

We now briefly outline a method of integrating edge diffraction modeling into the image source method [Pulkki et al. 2002]. Analogous to how specular reflection about a triangle is modeled by computing the image of the source with respect to the triangle, diffraction about an edge is modeled by computing the image of the source *with respect to the edge*. In the rest of the paper, we use the term “source” to refer to actual sound sources in the scene as well as image sources of any order.

The key idea is that the image source of a point source  $S$  with respect to diffracting edge  $E$  is that edge  $E$  itself (see Figure 3). This is based on the Huygens interpretation of diffraction [Medwin



**Algorithm 2** *AddNodes*(*node*, *IS*, *depth*)

---

```

{node is the current tree node, IS is an image source, depth is
the length of the current path}
if depth ≥ maxDepth then
    return node
else
    T ← triangles visible from IS
    E ← edges visible from IS
    for all t ∈ T do
        IIS ← image of IS about t
        child ← node for IIS
        add child as a child node of node
        child ← AddNodes(child, IIS, depth + 1)
    end for
    for all e ∈ E do
        IIS ← image of IS along e
        child ← node for IIS
        add child as a child node of node
        child ← AddNodes(child, IIS, depth + 1)
    end for
    return node
end if

```

---

**Algorithm 3** *ValidatePath*(*node*, *L*, *IR*)

---

```

{node is a node in the visibility tree, L is the listener, IR is the
impulse response}
if L is visible to image source in node then
    IR ← IR + contributions from path connecting all image
sources in nodes from node to root
    for all child ∈ children(node) do
        if image source in child is visible to image source in node
then
            IR ← IR + ValidatePath(child, L, IR)
        end if
    end for
end if
return IR

```

---

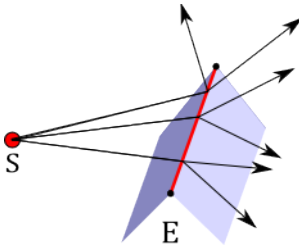


Fig. 3. Image source of a diffracting edge. Sound from source *S* scatters in all directions upon encountering diffracting edge *E*. *E* itself is therefore the image source of *S* about *E*. The fact that rays scatter in all directions from *E* implies that from-region visibility is required to compute all geometry reachable by these rays.

et al. 1982]. (Intuitively, one can think of modeling the diffraction about the edge in terms of infinitesimally small emitters located along the edge.) This means that image sources can now be points or line segments. It follows from the Huygens interpretation that the image of a line source  $E_1$  about a diffracting edge  $E_2$  is  $E_2$  (see Figure 4). Further note that the image of a point or line source

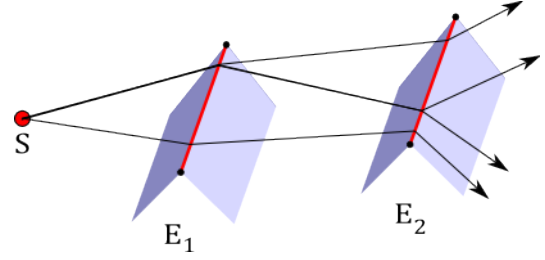


Fig. 4. Image sources for two successive diffractions. *S* is the source and  $E_1$  and  $E_2$  are diffracting edges.  $E_1$  induces a first-order diffraction image source along its length.  $E_2$  induces a second-order image source along its length.

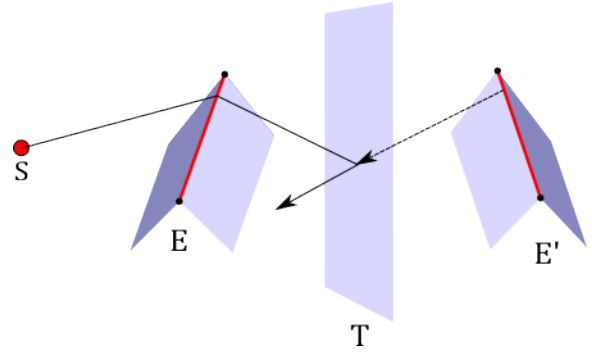


Fig. 5. Image sources for one diffraction followed by one specular reflection. *S* is the source and *E* is a diffracting edge. *T* is a specular reflector. *E* induces a diffraction image source along its length. This is reflected in the plane of *T* to give  $E'$ , which lies along the reflection of *E* in *T*.

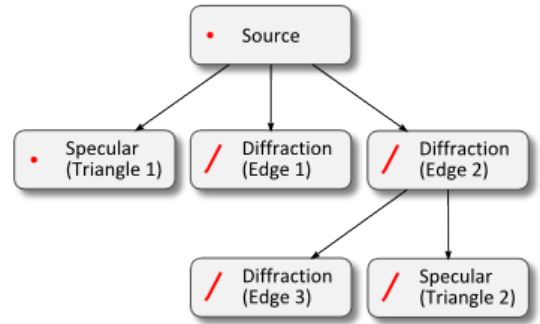


Fig. 6. Visibility tree. Each node is labelled with a triangle (for specular reflections) or an edge (for edge diffractions). Each path in this tree corresponds to a sequence of triangles and/or edges that can be encountered by a ray propagating from source to listener. The icon next to each node's label indicates whether the image source stored in the node is a point or line source.

$S_i$  about a planar specular reflector *T* is obtained by reflecting  $S_i$  across the plane of *T* (see Figure 5).

### 3.2 Visibility and Image Sources

In this section, we describe a modified image-source propagation algorithm, whose performance is accelerated using conservative

visibility computations. Note that we only need to compute image sources for a source  $S_i$  about triangles and/or edges that are visible to  $S_i$ . If  $S_i$  is a point source, this involves from-point visibility computation and conservative computation of the visible primitives at object-precision. If  $S_i$  is a line or edge source, however, we require from-region visibility computation, specifically, from-edge visibility computation. This visibility computation makes the BTM model much more complicated than the UTD model, which only computes visibility from a single point on the edge. In order not to miss potential propagation paths when computing image sources, we require object-precision from-region visibility, for which exact algorithms are complicated and slow. If we use image-space visibility algorithms they can either miss propagation paths or result in aliasing artifacts [Chandak et al. 2009].

In practice, most existing BTM implementations either approximate visibility information, or use overly conservative culling techniques. For example, the MATLAB Edge Diffraction toolbox is the state-of-the-art BTM implementation [Svensson 1999]. For any edge  $E$  formed by planes  $P_1$  and  $P_2$ , the toolbox implementation culls away edges whose both endpoints are behind both  $P_1$  and  $P_2$ . This is analogous to view frustum culling in graphics. In contrast, our approach uses a conservative from-region visibility algorithm to perform occlusion culling, so as to cull away additional geometry that is known to be invisible from  $E$ .

We use a two-step approach based on the image source method [Laine et al. 2009]. First, for a given source position  $S$ , we construct a visibility tree  $VT(S, k)$  upto a user-specified depth  $k$  (see Figure 6). Each path in  $VT(S, k)$  is a sequence of (upto  $k$ ) triangles and/or edges that a ray starting from  $S$  reflects and/or diffracts about as it reaches the listener at any position  $L$ . In other words, the paths in  $VT(S, k)$  partition the set of propagation paths from  $S$  to  $L$ , with each path  $P_t$  in  $VT(S, k)$  corresponding to an equivalence class  $R(P_t)$  of propagation paths between  $S$  and  $L$ . Next, given a listener position  $L$ , we traverse the visibility tree, and for each path  $P_t$  in  $VT(S, k)$ , we determine which of the propagation paths in  $R(P_t)$  are valid (i.e., unoccluded by other primitives) for the given source/listener pair. We refer to the second step of the process as *path validation*.

Each node in the tree corresponds to an image source  $S_i$ . Denote the node corresponding to  $S_i$  by  $N(S_i)$ . We begin by creating a single node  $N(S)$  corresponding to the source position  $S$ . The tree is then built recursively. To compute the children of  $N(S_i)$ , we compute the set of triangles  $T(S_i)$  and edges  $E(S_i)$  visible from  $S_i$ . For each  $t \in T(S_i)$  we reflect  $S_i$  about  $t$ , obtaining the reflection image source  $S_i^t$ , and construct the child node  $N(S_i^t)$ . For each  $e \in E(S_i)$ , we construct the child node  $N(e)$ . Note that computing  $T(S_i)$  and  $E(S_i)$  requires a from-point visibility query from  $S_i$  if it is a point source, or a from-region visibility query if it is a line or edge source. We stop construction of the tree beyond a given maximum depth. This maximum depth can be user specified in our implementation.

Note that the visibility tree essentially describes the search space of propagation paths that need to be considered when computing the impulse response at  $L$ . To ensure that we consider all possible diffraction paths between  $S$  and  $L$ , we need to ensure that we do not miss any of the visible edges when constructing the visibility tree. One way to ensure this is to assume each edge is visible from every other edge, or use the simple plane culling approach used by the MATLAB toolbox. However, this means that each node  $N(S_i)$  corresponding to an edge source  $S_i$  will have a very large number of children, many of which may not be reachable by a ray starting

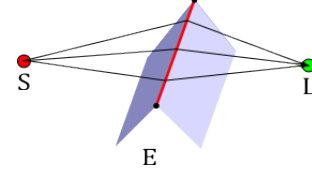


Fig. 7. Diffraction paths between source  $S$  and listener  $L$  across edge  $E$ . Note that here  $n = 3$  ray shooting tests are needed to validate the diffraction paths.

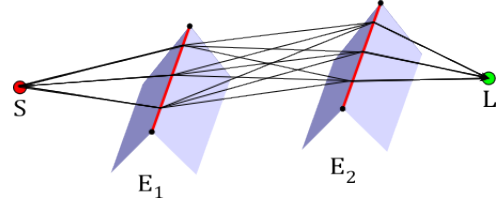


Fig. 8. Second order diffraction paths between source  $S$  and listener  $L$  across edges  $E_1$  and  $E_2$ . Note that here  $n = 3$  ray shooting tests are needed between  $S$  and  $E_1$  and between  $E_2$  and  $L$ , whereas  $n^2 = 9$  tests are required between  $E_1$  and  $E_2$ .

on  $S_i$ . This can dramatically increase the branching factor of the nodes in the tree, making higher-order paths almost impractical to compute. Therefore, we require conservative visibility algorithms for both from-point and from-region queries that are not overly conservative.

Another important point to note is that the tree must be reconstructed if the source moves. However, if the scene is static, all necessary from-region visibility information can be precomputed, allowing the tree to be rebuilt quickly. In the next section, we briefly describe the path validation process required to apply the BTM model for edge diffraction.

### 3.3 Path Validation

In this section, we present a method to validate the paths computed using the visibility tree described above. Specifically, we augment the prior methods by introducing a visibility function to accelerate the computations. After constructing the visibility tree for a given source position, the next step is to use the tree to find propagation paths between the source and the listener, and to compute contributions from these paths to the final impulse response at the listener position. We use the model described by Svensson et al. [1999], where the impulse response given a source at  $S$  and listener  $L$  and a single diffracting wedge is given by:

$$h(t) = -\frac{v}{4\pi} \int_{z_1}^{z_2} \delta\left(t - \frac{m(z) + l(z)}{c}\right) \frac{\beta(S, z, L)}{m(z)l(z)} dz \quad (1)$$

where  $v$  is the wedge index for the diffracting edge [Svensson et al. 1999],  $z_1$  and  $z_2$  are the endpoints of the edge,  $z$  is a point on the edge,  $m(z)$  is the distance between  $S$  and  $z$ ,  $l(z)$  is the distance between  $z$  and  $L$  and  $\beta(S, z, L)$  is essentially the diffraction attenuation along a path from  $S$  to  $z$  to  $L$ . We evaluate this integral by discretizing the edge into some  $n$  pieces and assuming that the integrand has a constant value over each piece (equal to its value at the

midpoint of the piece). For each edge piece this gives an attenuation of:

$$h_i = -\frac{v}{4\pi} \frac{V(S, z_i)V(z_i, L)\beta(S, z_i, L)}{m(z_i)l(z_i)} \Delta z_i \quad (2)$$

where  $h_i$  is the IR contribution caused by edge sample  $i$  with midpoint  $z_i$ . We augment the formulation of Svensson et al. [1999] by introducing  $V(x, y)$ , a Boolean valued visibility function which is true iff the ray from point  $y$  to point  $x$  is unoccluded by scene geometry. For second order diffraction, the corresponding attenuation is:

$$h_{ij} = \frac{v_1 v_2}{16\pi^2} V(S, z_i)V(z_i, z_j)V(z_j, L) \times \frac{\beta(S, z_i, z_j)\beta(z_i, z_j, L)}{m_1(z_i)m_2(z_i, z_j)l(z_j)} \Delta z_i \Delta z_j \quad (3)$$

where  $h_{ij}$  is the IR contribution from sample  $i$  on the first edge and sample  $j$  on the second edge, with midpoints  $z_i$  and  $z_j$  respectively. Here,  $v_1$  is the wedge index for the first edge and  $v_2$  is the wedge index for the second edge.

Given a path in the visibility tree which may contain any number of specular and/or diffraction nodes, we wish to use the Equations 2 and 3 to compute contributions to the final IR. For a given listener position  $L$ , we perform this step as follows:

- (1) We traverse each path in the tree in a bottom-up manner.
- (2) For each leaf node  $N(S_i)$ , we compute all valid propagation paths between  $S_i$  and  $L$ . For each internal node  $N(S_i)$  and its parent  $N(S_j)$ , we compute all valid propagation path segments between  $S_i$  and  $S_j$ .
- (3) For each valid path segment with endpoints  $p_i$  and  $p_j$ , we compute the corresponding delay  $\|p_j - p_i\|/c$ , distance attenuation  $1/\|p_j - p_i\|$ , specular attenuation  $\sigma = \sqrt{1 - \alpha}$  where  $\alpha$  is the frequency-dependent absorption coefficient of the reflecting triangle (if  $S_j$  is a specular node) and diffraction attenuation  $\beta(p_i, p_j, p_k)$  where  $p_k$  is the path endpoint corresponding to the parent of  $S_j$  (if  $S_j$  is a diffraction node).

In practice, these delays and attenuations are computed only if the corresponding visibility terms are nonzero. This check is performed using ray shooting between  $S_i$  and  $S_j$ . Ideally, we would like to compute the set of all unoccluded rays between  $S_i$  and  $S_j$ . (If  $S_j$  is formed by a specular reflector  $T$ , then we only consider the rays between  $S_i$  and  $S_j$  which intersect  $T$  and are unoccluded between  $S_i$  and their hit point on  $T$ .) If  $S_i$  and  $S_j$  are both point sources, this reduces to a simple ray shooting test. However, if either one is a line source, path validation reduces to from-region visibility computation.

In order to accurately compute contributions from each propagation path, we would ideally like to compute the exact visibility information. However, note that the BTM model computes the effect of diffraction about an edge in terms of a line integral over the edge. This integral must be discretized in order to compute impulse responses. We approximate the line integral using the midpoint method – by dividing the edge into  $n$  segments, and computing contributions due to paths passing through the midpoints of each segment. This method of integration allows us to use  $n$  ray

shooting tests (one for the midpoint of each of the  $n$  edge segments) to compute (approximate) visibility. Even though we use ray shooting and compute approximate visibility while computing IRs using the BTM model, it is necessary for us to compute conservative from-edge visibility when constructing the visibility tree. This is to ensure that no potential diffraction paths are missed. If an approximate visibility algorithm is used to construct the visibility tree, it may mark some edges that are visible from a given edge as invisible; this would lead to some diffraction paths being missed when computing IRs.

Observe that a propagation path is essentially a polyline which starts at the source, ends at the listener and whose intermediate vertices lie on triangles and/or edges in the scene. In the case of specular reflections only, path validation is performed using ray shooting to validate each segment of a polyline through the scene. If we also include one edge diffraction in the propagation path, we now need to validate  $n$  polylines through the scene, using  $n$  ray shooting tests for each image source along a path in the visibility tree. If we include a second edge, we need to validate  $n^2$  polylines, and so on. However, in this case, we do not need to perform  $n^2$  ray shooting tests for every image source along the path: only for image sources between the two diffracting edges (see Figures 7 and 8 for details). This is because there are  $n$  polylines from the source to the first edge, and  $n$  polylines from the second edge to the listener. Therefore the  $n^2$  polylines from the source to the listener share several common segments, which allows us to reduce the number of ray shooting tests required. By a similar argument, it can be shown that for third- and higher-order diffraction paths, the number of ray shooting tests required between any two image sources is at most  $O(n^2)$ , even though the total number of polylines is  $O(n^d)$  (where  $d$  is the number of diffracting edges in the path).

Once the validation step is complete and all contributions to the IR at the listener position have been computed, the next step is to render the final audio. We simply convolve the input sound signal with the computed impulse response to generate the output audio for a given listener position. To generate smooth audio for a moving listener, we interpolate between impulse responses at successive listener positions.

### 3.4 Cost Analysis

As previously discussed, our diffraction computation proceeds in two steps: first we compute mutually visible edge pairs, and next we compute IR contributions from each mutually visible edge pair. The cost of the first step, which we shall denote by  $C_{vis}$ , depends on the number of diffracting edges and the scene complexity (see Section 4 for details). Suppose the number of mutually visible edge pairs returned by the first step is  $N_{vis}$ . Then the cost per edge pair for the second step, which we shall denote by  $C_{IR}$ , depends on the edge sampling density (see Section 3.3 for details). Therefore, the total cost is:

$$C_{total} = C_{vis} + N_{vis}C_{IR} \quad (4)$$

$C_{IR}$  can be quite high, and therefore using an efficient, accurate from-region visibility algorithm allows us to reduce  $N_{vis}$  with a small overhead ( $C_{vis}$ ) and thus reduce the total cost. In this work, we concentrate on the use of visibility algorithms to reduce  $N_{vis}$ , and use a simple IR computation approach. Several techniques have been developed in the literature for efficient computation of IRs (which lower only  $C_{IR}$ ) [Calamia et al. 2009]; our approach can

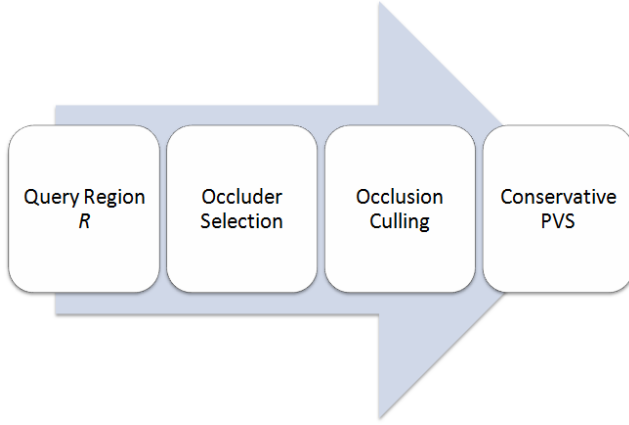


Fig. 9. Overview of our conservative from-region visibility approach. In the first step, we choose occluders for the query region  $R$ . Next, we use the occluders to compute which primitives are hidden from  $R$  by the occluders. The set of primitives not hidden by the occluders is the potentially visible set for  $R$ .

be modified to use these techniques to achieve improved overall performance.

#### 4. VISIBILITY COMPUTATION

In this section, we present our region-based visibility computation algorithm that is used to speed up the edge diffraction computation based on the visibility tree (as highlighted in Section 3). Specifically, we present a novel algorithm to compute the occluders from a given region and combine it with prior methods to compute the potentially visible set (PVS) of primitives from a given region at object-space precision. Figure 9 shows an overview of our visibility algorithm.

Formally, the from-region visibility problem can be described as follows. Given a convex region  $R \subset \mathbb{R}^3$  and a set of scene primitives  $\Pi$ , we wish to compute a subset of primitives  $\pi \subseteq \Pi$  such that every primitive  $p \in \Pi$  which is hit by a ray originating in  $R$  is included in  $\pi$ .  $\pi$  is called the *potentially visible set* (PVS) of  $R$ . The smallest such set is the *exact PVS*  $\pi_{exact}$  of  $R$ . Our algorithm returns a *conservative PVS*, i.e. a superset of the exact PVS ( $\pi \supseteq \pi_{exact}$ ).

Our visibility method can be divided into two steps: *occluder selection* for choosing primitives to be used as occluders for a given region  $R$ , and *occlusion culling* for computing the PVS of  $R$  given the set of occluders. Note that our algorithm is general and can be used to compute the PVS of any convex region, including line segments (edges), triangles and volumetric cells such as bounding boxes. In terms of sound rendering, we only use the algorithm to compute the PVS of the diffracting edges.

##### 4.1 Occluder Selection

The first step in computing the PVS of convex region  $R$  is to compute the potential occluders for  $R$ . One option would be to simply use every primitive in the scene as an occluder, and use an occlusion culling algorithm that handles occluder fusion. In an ideal scenario,

such an approach would result in a PVS that is as close as possible to  $\pi_{exact}$ . However, the main issue with such an approach, which limits its practical application, is that the cost of occlusion culling is typically a function of the number of occluders [Chhugani et al. 2005]. Most prior work on occluder selection uses heuristics based on distance, solid angles, or area of primitives [Coorg and Teller 1997; Hudson et al. 1997; Durand et al. 2000; Koltun and Cohen-Or 2000]. Although these methods compute a subset of  $\Pi$  to be used as occluders, they are unable to exploit the connectivity information of primitives to find any arbitrary set of connected triangles as occluders. If we are able to combine small occluders into large occluders, it can improve the culling efficiency of the visibility algorithm.

Thus, we propose a novel from-region occluder selection algorithm which exploits the connectivity information between scene primitives whenever feasible. Our approach is general and applicable to all kinds of models including “polygon soup” models. We make no assumptions about the model or the connectivity of the polygons. (In our implementation, the models are assumed to be triangulated, however, this is not a restriction imposed by our algorithm.) If the model connectivity information is given or can be extracted, our algorithm can exploit that information to compute large occluders formed by connected sets of primitives.

Our technique can be viewed as a generalization of the conservative from-point visibility technique used in the FastV algorithm [Chandak et al. 2009]. FastV computes from-point visibility by constructing a cubical box around the query point  $R$ , then subdividing each of its faces into multiple quad patches  $Q$  (where the number of quad patches can be user-specified), and then constructing frusta  $F(R, q)$  from each quad patch  $q \in Q$  and  $R$  (see Figure 10). Each of these frusta is used to compute which portions of the scene are visible from the query point that use the relevant patch as the viewport. Formally, for each  $q \in Q$  we wish to determine the set of primitives  $p \in \Pi$  such that there exists a ray from  $R$  to some point on  $p$  which passes through  $q$ .

Given a frustum  $f = F(R, q)$  (defined by its corner rays), the FastV algorithm tries to compute a *blocker* for  $f$ . In the context of FastV, a blocker is defined as a connected set of triangles such that any convex combination of the corner rays of  $f$  intersects some triangle in the blocker. FastV traverses the scene hierarchy, and whenever a triangle  $T$  is found that intersects  $f$ , it uses the connectivity information associated with  $T$  to determine if some set of triangles connected to  $T$  can also be used as a blocker for  $f$ . It is possible that there may be no such triangles. Therefore, once the traversal is completed, FastV returns at most one blocker for  $f$  and zero or more connected sets of triangles in front of the blocker which do not completely block  $f$ .

Consider generalizing the frustum construction approach of FastV to the from-region case (i.e., now  $R$  can be any convex region). We compute a fattened oriented bounding box (where the amount of “fattening” can be user-specified) that encloses  $R$  and subdivide its faces into a user-specified number of quad patches  $Q$ . The next step is to determine the set of primitives  $p$  such that there exists at least one ray from some point  $r \in R$  to  $p$  which passes through  $q$ . Put another way, we wish to determine all points from which  $R$  is partially visible through  $q$ . This corresponds to the region in front of  $q$  and bounded by the set  $S$  of *separating planes* constructed between  $R$  and  $q$  [Coorg and Teller 1997] (see Figure 11).

Note that we orient the separating planes such that  $Q$  lies in the positive half-space (interior) defined by each separating plane  $s \in S$ .



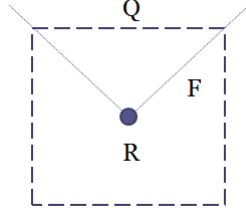


Fig. 10. Frustum construction performed by FastV. Given a query point  $R$ , we construct an axis-aligned box around it and divide the faces of the box into quad patches, one of which,  $Q$ , is shown in the figure. Given  $R$  and  $Q$ , we then trace a frustum  $F$  to compute the PVS for  $R$ .

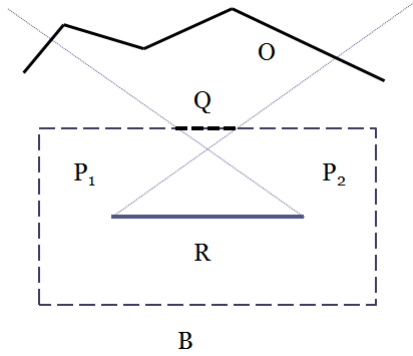


Fig. 11. Separating frustum construction, in 2D. Given a line segment  $R$ , we construct a fattened bounding box  $B$ , and divide its boundary into line segment patches, one of which is  $Q$ . We construct separating planes  $P_1$  and  $P_2$  between  $R$  and  $Q$ , and trace the frustum bounded by these planes and oriented such that  $Q$  is in the interior of the frustum. Here  $O$  is a blocker for the separating frustum, and is used as an occluder for  $R$ .

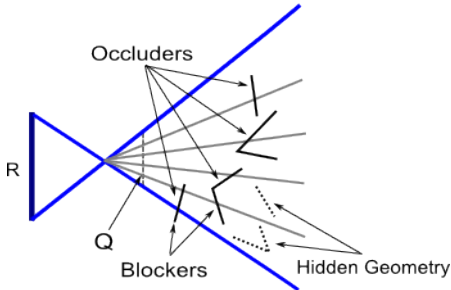


Fig. 12. Occluder selection in 2D. The bright blue lines are the corner rays of the separating frustum between query region  $R$  and quad patch  $Q$ . The grey lines indicate corner rays of sub-frusta formed by uniform frustum subdivision. Primitives chosen as occluders are shown as solid line segments, primitives hidden by the occluders are shown as dotted line segments. Some of the occluders are frustum blockers, and these are also marked in the figure.

We then construct a *separating frustum*  $f = F(R, q)$  bounded by  $S$ . The separating frustum need not be pyramidal; it is defined as the intersection of half-spaces bounded by the separating planes. We could use view frustum culling techniques to cull  $\Pi$  to  $f$  to estimate the PVS of  $R$ . However, this approach may compute a PVS  $\pi$  such that there exist primitives  $p_1, p_2 \in \pi$  where  $p_1$  occludes  $p_2$

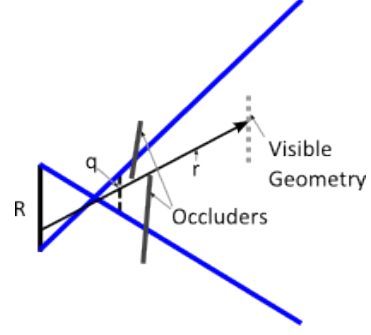


Fig. 13. Accuracy issues with using from-point algorithms with separating frusta. The figure shows an example scenario where FastV would be unable to compute a conservative PVS. If FastV is used to process the separating frustum formed by region  $R$  and quad patch  $q$ , the indicated occluders will be marked as visible. However, there could be geometry behind the occluders which can be reached by a ray originating on  $R$ , but which may be marked invisible by FastV depending on frustum subdivision level.

from  $R$ , and the resulting PVS would be too conservative. Instead, we use FastV to trace  $f$  (see Figure 11). (Note that if  $R$  is in fact a single point, our occluder selection algorithm reduces to FastV.)

Ideally, we would like to trace all the rays that start on  $R$  and pass through  $q$ , and the set of primitives reached would approach  $\pi_{exact}$ . However, tracing  $f$  using FastV computes a *subset* of triangles visible from  $R$  through  $Q$  (i.e., computes  $\pi \subseteq \pi_{exact}$ ). This subtle difference between the from-point and from-region case occurs because using FastV with a separating frustum for a region  $R$  is not guaranteed to find all geometry reachable by rays starting on  $R$  (for an example, see Figure 13) for a given frustum subdivision level. Therefore, after occluder selection, we use a conservative occlusion culling algorithm to compute a superset of the exact PVS.

Tracing  $f = F(R, q)$  using FastV can return a blocker for  $f$ . This blocker is a connected set of triangles such that any ray originating on  $R$  and passing through  $q$  intersects the blocker. Therefore, we use all blockers returned by FastV as occluders. However, it is possible that FastV may be unable to find a blocker for  $f$ . In such a case, we use the connected sets of triangles computed by FastV during scene traversal as occluders (see Figure 12 for an example).

## 4.2 PVS Computation

Given a set of occluders for  $R$ , the next step is to perform occlusion culling to compute the PVS of  $R$ . Ideally, we would like to determine the umbra of an occluder  $o$  with respect to  $R$ . Unfortunately, the boundary of an exact umbra is bounded by curved surfaces [Teller 1992]. A common workaround is to compute a *shadow frustum* bounded by these curved surfaces, and use it to determine a subset of triangles occluded by  $o$  (thus computing a superset of the exact PVS for  $R$ ). The shadow frustum is bounded by the *supporting planes* between  $R$  and  $o$  [Chugani et al. 2005], and can be easily computed.

We can use any existing object-precision technique for occlusion culling, as long as it guarantees that the resulting PVS is conservative. Several methods that fit these requirements exist in the literature [Durand et al. 2000; Chugani et al. 2005]. In our implementation, we have used a simple CPU-based frustum culling method. For each occluder  $o$ , we compute the shadow frustum  $S(o, R)$  of

$o$  from  $R$  and mark all primitives behind  $o$  and completely contained in  $S(o, R)$  as occluded from  $R$ . Once all shadow frusta have been processed in this manner, the primitives not marked hidden are added to the PVS of  $R$ .

### 4.3 Cost Analysis

In this section we present a simple cost model for from-region visibility algorithms. Most from-region visibility algorithms can be decomposed into two steps: (a) Occluder Selection and (b) PVS Computation. These two steps are described in Section 4.1 and Section 4.2 for our approach. Thus, for a given region,  $R$ , the cost of from-region visibility from  $R$  depends on the cost of the previous two steps.

$$T_{FR}(R) = T_{OS}(R) + T_{PVS}(R, O) \quad (5)$$

Where  $T_{FR}(R)$ ,  $T_{OS}(R)$ , and  $T_{PVS}(R, O)$  are the computation cost of from-region visibility, occluder selection, and PVS computation from region  $R$ . The PVS computation step depends on the occluder set  $O$  computed by the occluder selection step. We choose a very simplistic cost model dependent only upon the computation times of occluder selection and PVS computation steps as this is sufficient for comparison with other visibility approaches (see Section 4.4). We exclude discussion on simple heuristic-based algorithms for occluder selection. These algorithms choose a few occluders which are likely to occlude a large portion of the scene but such occluders are typically a small fraction of occluders that contribute to occlusion from a region for a scene [Wonka et al. 2000] and can lead to a highly conservative PVS.

### 4.4 Comparison

The main application of our visibility algorithm is finite edge diffraction computation for sound rendering. We need to find all potentially visible edges from a given edge to compute higher order diffraction from the given edge. Missing edges which are visible from the given edge leads to a discontinuous sound field around the missed edges. The discontinuous sound field could lead to artifacts in sound rendering and this is unacceptable for our application. This fits very well into the kind of applications described by Wonka et al. [2000] where non-conservative (approximate) visibility algorithms, though beneficial, are not tolerable. Exact from-region visibility algorithms are prohibitively expensive for our application. Thus, we present a comparison of our approach with conservative from-region algorithms [Cohen-Or et al. 2003] in this section with special focus on occluder selection choices of these algorithms.

Efficient algorithms have been developed for computing conservative from region visibility for 2D and 2.5D [Koltun and Cohen-Or 2000; Koltun et al. 2001; Wonka et al. 2000]. Schaufler et al. [2000] can compute conservative from region visibility for 3D scenes but require the occluders in the scene to be volumetric. Our approach is a generic 3D visibility algorithm and does not impose restrictions on the scene geometry. Thus, the above approaches are not relevant for comparison with our approach.

Extended Projections [Durand et al. 2000] compute underestimated projections of occluders and overestimated projections of occludees from any viewpoint inside the region to perform occlusion culling. Thus, the PVS computation cost  $T_{PVS}(R, O)$  depends linearly on the size of the occluder set and the projection of the occluders is the bottleneck of Extended Projections. The occluder se-

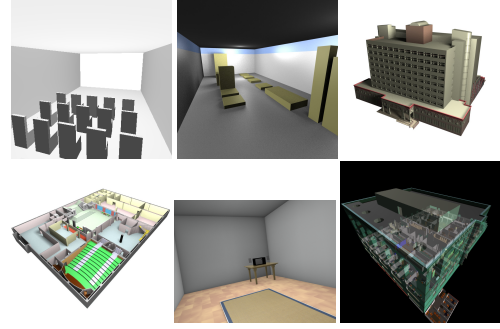


Fig. 14. Benchmarks. Clockwise from top left: (a) Room (876 triangles) (b) Factory (170 triangles) (c) Building (69K triangles) (d) Soda Hall (1.5M triangles) (e) House (1K triangles) (f) Floor (7.3K triangles).

lection algorithm employed by Extended Projections computes occluders based on solid angle heuristics which could lead to highly conservative PVS in addition to a non-optimal set of occluders for a given size of occluder set [Koltun and Cohen-Or 2000].

vLOD [Chhugani et al. 2005] computes a shadow frustum for each occluder and finds an optimal projection point to compute a shrunk shadow frustum to determine conservative visibility. Computing an optimal projection point is formulated as a convex quadratic optimization problem which depends at least linearly on the size of the occluder set. Furthermore, the occlusion culling step in vLOD can benefit from the connected occluders computed by our occluder selection algorithm.

## 5. RESULTS

In this section, we present experimental results on sound propagation and from-region visibility. We compare our sound propagation system with the state-of-the-art to highlight the benefits of using from-region visibility when computing sound propagation paths. Figure 14 shows the scenes we use to benchmark our code. The Room, Factory and House scenes are used to benchmark visibility tree construction. The Building, Floor and Soda Hall examples are complex scenes used to benchmark our occluder selection algorithm. Figure 17 shows some examples of diffraction paths computed by our algorithm. All of our tests were performed on an Intel Xeon X5560 workstation with 4GB RAM, running Windows Vista. Our implementation is written in C++ and uses SSE instructions to achieve high performance. All timings are reported for a single CPU core.

Table I shows the breakdown of time spent in each step of our algorithm. It is evident from the table that the costliest step of our algorithm is the final IR computation. Computing from-region visibility and constructing the visibility tree is much faster by comparison. Moreover, occluder selection is much quicker than occlusion culling; this allows us to use our occluder selection algorithm to reduce the time spent in the occlusion culling step. Note that all timings in this section are reported for the following values of parameters used by our algorithm: upto 2 orders of specular reflection; upto 2 orders of edge diffraction;  $4 \times 4$  quad subdivision and  $4 \times 4$  uniform frustum subdivision [Chandak et al. 2009].

**Visibility Tree Construction** We first demonstrate the advantage of using from-region visibility in our BTM-based sound propagation system. We compare the performance of our visibility tree con-

Table I. Performance of individual steps of our algorithm.

| Scene   | Occluder Selection (ms) | Occlusion Culling (ms) | Visibility Tree (ms) | IR Computation (s) |
|---------|-------------------------|------------------------|----------------------|--------------------|
| Factory | 3.6                     | 7.9                    | 141.0                | 23.9               |
| Room    | 8.9                     | 93.3                   | 747.6                | 10.4               |
| House   | 14.6                    | 75.0                   | 1045.6               | 24.3               |

Column 1 shows the average time taken for occluder selection per diffracting edge. Column 2 shows the average time taken for occlusion culling (PVS computation) per diffracting edge. Column 3 shows the time spent in constructing the visibility tree, averaged over multiple source positions. Column 4 shows the time taken to compute the final IR, averaged over multiple source and listener positions.

struction step (using from-region visibility) against visibility tree construction using only the simple culling approach used in the MATLAB Edge Diffraction toolbox [Svensson 1999] (as implemented in C++). We compare the time required to build the visibility tree as well as the size of the tree constructed for each approach. Our results are summarized in Table II.

When numerically evaluating the BTM integral, we divide each edge into 44K samples [Calamia et al. 2009]. Evaluating the visibility functions (Equations 2 and 3) for each of these 44K samples using ray shooting would be very time-consuming. Therefore, we subsample the edges and perform ray shooting visibility tests only between these subsampled points. The edge sampling densities reported in Table II refer to these subsampled points.

The table clearly highlights the importance of from-region occlusion culling in the BTM model. In the absence of occlusion culling, the size of the visibility tree grows very rapidly with depth. Our approach uses occlusion culling to reduce the branching factor of the nodes of the visibility tree. Reducing the size of the tree in turn implies faster validation of diffraction paths using the BTM model. Note that the speedup numbers were measured for the particular edge sampling densities specified in the table. However, the speedup numbers compare the values of  $N_{vis}C_{IR}$  (see Section 3), where  $N_{vis}$  varies with the visibility algorithm chosen. Since  $C_{IR}$  (which depends on the edge sampling density) does not vary with choice of visibility algorithm, the speedup numbers remain roughly constant for different values of edge sampling density.

Figure 15 shows the average percentage of total triangles (and diffracting edges) visible from the diffracting edges in various benchmark scenes. These plots clearly show that even in simple scenes which are typically used for interactive sound propagation, occlusion culling helps reduce the complexity of the visibility tree computed by our algorithm by a factor of 2 to 4.

**Occluder Selection for From-Region Visibility** We now turn to the performance of our from-region visibility implementation. Note that the following results are reported for from-triangle visibility. We report the running times of our occluder selection step per triangle in Table III. The table also reports the average number of triangles in each occluder. This demonstrates how our occluder selection algorithm is able to effectively combine connected triangles into larger occluders. This results in larger occluders, which can potentially allow more triangles to be culled. Moreover, the computational cost of state-of-the-art from-region occlusion culling algorithms tends to increase with an increase in the number of occluders. The time required for such computations can be reduced by using fewer, larger occluders formed by connected sets of triangles, such as those selected by our algorithm.

Table IV compares the total running time for from-region visibility (occluder selection and occlusion culling) and the resulting PVS sizes when our occlusion culling implementation is provided with

Table III. Performance of our occluder selection algorithm for various benchmarks.

| Scene     | Triangles | Occluder Selection |                       |
|-----------|-----------|--------------------|-----------------------|
|           |           | Time (s)           | Avg tris per occluder |
| Floor     | 7.3K      | .12                | 6.0                   |
| Building  | 69K       | 1.3                | 3.0                   |
| Soda Hall | 1.5M      | 14.8               | 6.7                   |

All timings are reported for occluder selection for a single triangle (averaged over multiple triangles). The last column indicates the average size of occluders (in no. of triangles) returned by the occluder selection algorithm.

occluders computed using three approaches: no occluder selection (i.e., using all primitives as occluders), area-ratio heuristics [Koltun and Cohen-Or 2000], and our occluder selection algorithm based on tracing separating frusta. The table clearly shows that using our occluder selection algorithm significantly reduces total time spent in visibility computation as compared to the other approaches, at the cost of a relatively small increase in PVS size. Note that when selecting occluders using the area-ratio heuristic, we evaluate the area-ratio for each primitive and choose all primitives whose scores are greater than or equal to the median score as occluders.

**Impulse Responses and Comparisons** We have implemented the line integral formulation of the BTM model [Svensson et al. 1999] for performing path validation and computing impulse responses. The crucial parameter in the validation step is the number of samples each edge is divided into. A higher number of samples per edge results in more accurate evaluation of the BTM integral at a higher computational cost. Figure 16 shows impulse responses computed for diffraction about a simple double wedge for increasing numbers of samples per edge. As can be seen from the figure, increasing the number of samples causes the IRs to converge to the reference IR computed by the MATLAB toolbox [Svensson 1999] (also shown in Figure 16). Although we have used a simplistic approach for calculating IRs in our implementation, the variation of IR accuracy with edge sampling strategy and sampling density has been studied in the literature [Calamia and Svensson 2005; Calamia and Svensson 2007].

Further note that although the computational cost of the BTM model remains higher than that of the UTD model, it has been shown [Svensson et al. 1999] that the BTM model is more accurate than UTD model at low frequencies, where diffraction plays an important role. Furthermore, the UTD approach does not model the diffraction contributions in regions where the listener is in line-of-sight of the source, whereas the BTM approach does. At low frequencies, numerical methods can be used to capture diffraction effects, but the complexity scales with the volume of the scene, as opposed to BTM-based methods whose complexity scales with the number of diffracting edges. Moreover, combining a numerical acoustics algorithm with geometric acoustics techniques for high frequency simulations remains a challenging problem, whereas the

Table II. Advantage of using conservative from-region visibility for second order edge diffraction.

| Scene   | Triangles | Edges | Second order diffraction paths in tree |         |                | BTM validation speedup |         |
|---------|-----------|-------|--|---------|----------------|------------------------|---------|
|         |           |       | Our method                             | Toolbox | Size reduction | Edge intervals         | Speedup |
| Factory | 170       | 146   | 4424                                   | 12570   | 2.84           | $10 \times 10$         | 1.93    |
| Room    | 876       | 652   | 43488                                  | 181314  | 4.17           | $5 \times 5$           | 3.23    |
| House   | 1105      | 751   | 133751                                 | 393907  | 2.95           | $5 \times 5$           | 13.74   |

Columns 4–6 demonstrate the benefit of using from-region visibility to cull away second order diffraction paths between mutually invisible edges. The last column shows the speedup caused by this reduction in the size of the visibility tree. Column 7 refers to the number of rays shot per edge and the number of integration intervals corresponding to each ray. For example,  $5 \times 5$  refers to 5 rays shot per edge and a total of 25 integration intervals, with each ray shooting test used to compute the visibility term for 5 consecutive integration intervals.

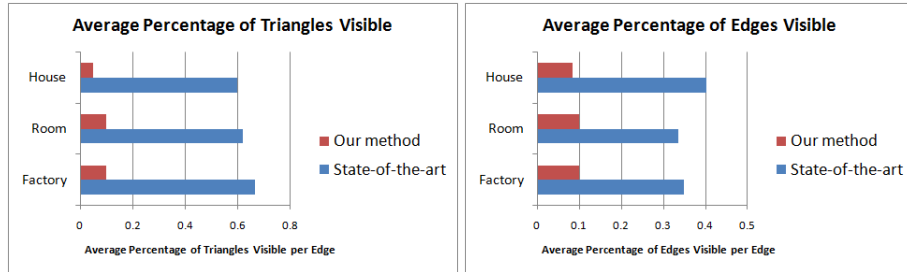


Fig. 15. Average amount of visible geometry returned by our approach as compared to the state-of-the-art for various benchmarks. The horizontal axis measures the fraction of visible geometry (triangles or edges, respectively) averaged over all edges in the scene. Smaller is better.

BTM approach can easily be combined with the image source method to compute accurate diffraction effects.

Table II also shows the speedup obtained in the validation and IR computation step as a result of using conservative from-region visibility when constructing the visibility tree. As the table demonstrates, even for a very unoptimized implementation running on a single core, using conservative visibility algorithms can offer a significant performance advantage over state-of-the-art BTM-based edge diffraction modeling methods.

## 6. CONCLUSION

We have demonstrated the importance of conservative, object-space accurate from-region visibility in a geometric sound propagation system that can model specular reflections and edge diffractions. This is used to develop a fast sound propagation system. The approach is based on the image source method, and integrates edge diffraction into the image source framework. Edge diffractions are modeled using the Biot-Tolstoy-Medwin model. The set of potential propagation paths that need to be tested for validity is significantly reduced using fast conservative object-space from-region visibility techniques. This greatly accelerates the process of computing sound propagation paths and their contributions to the impulse response at the listener, leading to significant performance improvements over state-of-the-art geometric algorithms for modeling higher-order edge diffraction.

Our from-region visibility algorithm uses a novel, systematic occluder selection method that is fast and can assemble connected triangles into a single larger occluder. This allows for efficient occlusion culling using state-of-the-art techniques. Our approach is easy to parallelize and scales well on multi-core architectures. The modularity of our technique allows us to use our occluder selection algorithm with any from-region occlusion culling algorithm

and gain the benefits of combining adjacent triangles into single occluders.

### 6.1 Limitations

Our approach has several limitations. It is possible that in the absence of large primitives that can be used as occluders, our algorithm would have to trace a large number of small frusta in order to select occluders, which could adversely affect its performance.

The BTM model is computationally intensive, and to the best of our knowledge, there exist no implementations of third- or higher-order edge diffraction based on it. However, there do exist special cases where it is necessary to model very high orders of edge diffraction; one example is the case of sound diffracting around the highly tessellated surface of a large pillar.

Note that the formulation of Equations 2 and 3 has been developed for infinitely rigid wedges [Svensson et al. 1999]. In our implementation, we combine diffraction effects modeled using Equations 2 and 3 with specular reflections which model partially absorbing surfaces. The accuracy of such a combination remains to be studied.

### 6.2 Future Work

There are many possible avenues for future work. Our current implementation of our from-region visibility algorithm uses a simple object-space frustum culling technique for occlusion culling. This can cause it to miss cases of occluder fusion due to disconnected occluders. One possibility is to use conservative rasterization methods [Chugani et al. 2005; Akenine-Möller and Aila 2005], which may be able to fuse such occluders and thereby result in a smaller PVS from a given region. Moreover, the occluder selection step itself can be implemented on the GPU for additional performance gains.



Table IV. Benefit of our occluder selection algorithm.

| Scene   | Triangles | No Occluder Selection |          | Area Ratio Heuristic |          | Tracing Separating Frusta |          |
|---------|-----------|-----------------------|----------|----------------------|----------|---------------------------|----------|
|         |           | Time (ms)             | PVS Size | Time (ms)            | PVS Size | Time (ms)                 | PVS Size |
| Factory | 170       | 15.2                  | 64       | 14.9                 | 64       | 11.5                      | 69       |
| Room    | 876       | 240                   | 356      | 241.4                | 356      | 102                       | 379      |
| House   | 1150      | 192                   | 209      | 112.2                | 261      | 90                        | 350      |

Average computation time and PVS size when using different occluder selection algorithms. “No Occluder Selection” refers to using all triangles as occluders. “Area Ratio Heuristic” refers to the use of Koltun et al.’s [2000] heuristic approach. “Tracing Separating Frusta” refers to our algorithm described in Section 4.1. Columns 3, 5 and 7 compare total running times for computing from-triangle visibility averaged over all triangles in the respective scenes. Columns 4, 6 and 8 compare the average PVS size per triangle.

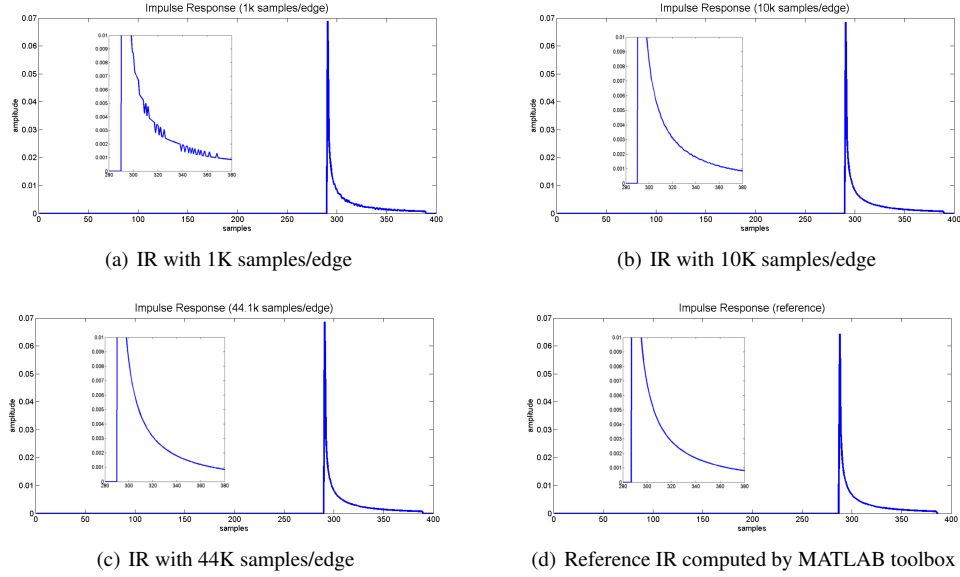


Fig. 16. Accuracy of impulse responses computed by our system for first order diffraction about a single finite wedge. Parts (a)–(c) show the variation in the IR with increasing number of samples per edge. As the sampling increases, the IR approaches the reference IR computed by the MATLAB toolbox, shown in part (d).

While our visibility tree construction step can construct paths of the form  $source \rightarrow \dots \rightarrow diffraction \rightarrow specular \rightarrow \dots \rightarrow diffraction \dots$ , we discard such paths and do not compute IR contributions from them. Similarly, we discard paths with three or more edge diffractions. It would be a simple task to perform the visibility checks required to compute which such paths are valid. However we are not aware of any BTM-based method for computing attenuations which can handle specular reflections between two edge diffractions, and therefore cannot compute contributions from such paths.

We use a simple midpoint method to evaluate the BTM integral and compute edge diffraction contributions to the final impulse response. However, the BTM integrand has poles which cannot be integrated across [Svensson and Calamia 2006; Calamia and Svensson 2007]. Our simple integration method does not account for these poles, and may integrate across them, leading to errors in the impulse response. Moreover, we do not cull diffraction contributions based on their amplitude. It has been shown that prioritizing contributions with large amplitudes and culling contributions with small amplitude can lead to a significant performance gain for first-order diffraction [Calamia et al. 2009]. It would be worthwhile to extend this idea to second-order diffraction.

## REFERENCES

- AKENINE-MÖLLER, T. AND AILA, T. 2005. Conservative and tiled rasterization using a modified triangle setup. *Journal of Graphics, GPU, and Game Tools* 10, 3, 1–8.
- ALLEN, J. B. AND BERKLEY, D. A. 1979. Image method for efficiently simulating small-room acoustics. *The Journal of the Acoustical Society of America* 65, 4, 943–950.
- ANTONACCI, F., FOCO, M., SARTI, A., AND TUBARO, S. 2004. Fast modeling of acoustic reflections and diffraction in complex environments using visibility diagrams. In *Proceedings of 12th European Signal Processing Conference (EUSIPCO '04)*. 1773–1776.
- BEGAULT, D. R. 1994. *3-D sound for virtual reality and multimedia*. Academic Press Professional, Inc., San Diego, CA, USA.
- BIOT, M. A. AND TOLSTOY, I. 1957. Formulation of wave propagation in infinite media by normal coordinates with an application to diffraction. In *Ocean Acoustics: Theory and Experiment in Underwater Sound*. Acoustical Society of America, 305–330.
- BITTNER, J., HAVRAN, V., AND SLAVIK, P. 1998. Hierarchical visibility culling with occlusion trees. In *CGI '98: Proceedings of the Computer Graphics International 1998*. IEEE Computer Society, Washington, DC, USA, 207.

- BITTNER, J., MATTAUSCH, O., WONKA, P., HAVRAN, V., AND WIMMER, M. 2009. Adaptive global visibility sampling. In *SIGGRAPH '09: ACM SIGGRAPH 2009 papers*. ACM, New York, NY, USA, 1–10.
- BITTNER, J. AND WONKA, P. 2003. Visibility in computer graphics. *Environment and Planning B: Planning and Design* 30, 5, 729–756.
- CALAMIA, P., MARKHAM, B., AND SVENSSON, U. P. 2009. Diffraction culling for virtual-acoustic simulations. *The Journal of the Acoustical Society of America* 125, 4, 2586–2586.
- CALAMIA, P. AND SVENSSON, U. P. 2005. Edge subdivision for fast diffraction calculations. In *Proc. 2005 IEEE Workshop on Applications of Signal Processing to Audio and Acoustics*. 187–190.
- CALAMIA, P. T. AND SVENSSON, U. P. 2007. Fast time-domain edge-diffraction calculations for interactive acoustic simulations. *EURASIP J. Appl. Signal Process.* 2007, 1, 186–186.
- CALAMIA, P. T., SVENSSON, U. P., AND FUNKHOUSER, T. A. 2005. Integration of edge diffraction calculations and geometrical-acoustics modeling. In *Proceedings of Forum Acusticum 2005*.
- CHAMBERS, J. P. AND BERTHELOT, Y. H. 1994. Time-domain experiments on the diffraction of sound by a step discontinuity. *The Journal of the Acoustical Society of America* 96, 3, 1887–1892.
- CHANDAK, A., ANTANI, L., TAYLOR, M., AND MANOCHA, D. 2009. FastV: From-point visibility culling on complex models. *Computer Graphics Forum* 28, 1237–1246(10).
- CHANDAK, A., LAUTERBACH, C., TAYLOR, M., REN, Z., AND MANOCHA, D. 2008. Ad-frustum: Adaptive frustum tracing for interactive sound propagation. *IEEE Transactions on Visualization and Computer Graphics* 14, 6, 1707–1722.
- CHHUGANI, J., PURNOMO, B., KRISHNAN, S., COHEN, J., VENKATASUBRAMANIAN, S., JOHNSON, D. S., AND KUMAR, S. 2005. vLOD: High-fidelity walkthrough of large virtual environments. *IEEE Transactions on Visualization and Computer Graphics* 11, 1, 35–47.
- CISKOWSKI, R. AND BREBBIA, C. 1991. *Boundary element methods in acoustics*. Computational Mechanics Publications and Elsevier Applied Science.
- COHEN-OR, D., CHRYSANTHOU, Y., SILVA, C., AND DURAND, F. 2003. A survey of visibility for walkthrough applications. *Visualization and Computer Graphics, IEEE Transactions on* 9, 3 (july-sept.), 412–431.
- COORG, S. AND TELLER, S. 1997. Real-time occlusion culling for models with large occluders. In *SI3D '97: Proceedings of the 1997 symposium on Interactive 3D graphics*. ACM, New York, NY, USA, 83–ff.
- DALENBÄCK, B. 1996. Room acoustic prediction based on a unified treatment of diffuse and specular reflection. *The Journal of the Acoustical Society of America* 100, 2, 899–909.
- DURAND, F., DRETTAKIS, G., AND PUECH, C. 1996. The 3d visibility complex: a new approach to the problems of accurate visibility. In *Proceedings of the eurographics workshop on Rendering techniques '96*. Springer-Verlag, London, UK, 245–256.
- DURAND, F., DRETTAKIS, G., AND PUECH, C. 1997. The visibility skeleton: a powerful and efficient multi-purpose global visibility tool. In *SIGGRAPH '97: Proceedings of the 24th annual conference on Computer graphics and interactive techniques*. ACM Press/Addison-Wesley Publishing Co., New York, NY, USA, 89–100.
- DURAND, F., DRETTAKIS, G., THOLLOT, J., AND PUECH, C. 2000. Conservative visibility preprocessing using extended projections. In *SIGGRAPH '00: Proceedings of the 27th annual conference on Computer graphics and interactive techniques*. ACM Press/Addison-Wesley Publishing Co., New York, NY, USA, 239–248.
- FUNKHOUSER, T., CARLBOM, I., ELKO, G., PINGALI, G., SONDH, M., AND WEST, J. 1998. A beam tracing approach to acoustic modeling for interactive virtual environments. In *Proc. of ACM SIGGRAPH*. 21–32.
- GHALI, S. 2001. A survey of practical object-space visibility algorithms. In *SIGGRAPH Tutorial Notes*.
- GIGUS, Z., CANNY, J., AND SEIDEL, R. 1991. Efficiently computing and representing aspect graphs of polyhedral objects. *IEEE Trans. Pattern Anal. Mach. Intell.* 13, 6, 542–551.
- HECKBERT, P. S. AND HANRAHAN, P. 1984. Beam tracing polygonal objects. *SIGGRAPH Comput. Graph.* 18, 3, 119–127.
- HUDSON, T., MANOCHA, D., COHEN, J., LIN, M., HOFF, K., AND ZHANG, H. 1997. Accelerated occlusion culling using shadow frusta. In *SCG '97: Proceedings of the thirteenth annual symposium on Computational geometry*. ACM, New York, NY, USA, 1–10.
- KAPRALOS, B., JENKIN, M., AND MILIOS, E. 2004. Sonel mapping: acoustic modeling utilizing an acoustic version of photon mapping. In *IEEE International Workshop on Haptics Audio Visual Environments and their Applications (HAVE 2004)*. 2–3.
- KOLTUN, V., CHRYSANTHOU, Y., AND COHEN-OR, D. 2001. Hardware-accelerated from-region visibility using a dual ray space. In *Proceedings of the 12th Eurographics Workshop on Rendering Techniques*. Springer-Verlag, London, UK, 205–216.
- KOLTUN, V. AND COHEN-OR, D. 2000. Selecting effective occluders for visibility culling. In *Eurographics Short Presentations*.
- KOUYOUMJIAN, R. G. AND PATHAK, P. H. 1974. A uniform geometrical theory of diffraction for an edge in a perfectly conducting surface. *Proc. of IEEE* 62, 1448–1461.
- KROKSTAD, A., STROM, S., AND SORSDAL, S. 1968. Calculating the acoustical room response by the use of a ray tracing technique. *Journal of Sound and Vibration* 8, 1 (July), 118–125.
- KUTTRUFF, H. 1991. *Room Acoustics*. Elsevier Science Publishing Ltd.
- LAINE, S., SILTANEN, S., LOKKI, T., AND SAVIOJA, L. 2009. Accelerated beam tracing algorithm. *Applied Acoustic* 70, 1, 172–181.
- LAUTERBACH, C., CHANDAK, A., AND MANOCHA, D. 2007. Adaptive sampling for frustum-based sound propagation in complex and dynamic environments. In *Proceedings of the 19th International Congress on Acoustics*.
- LAW, F.-A. AND TAN, T.-S. 1999. Preprocessing occlusion for real-time selective refinement. In *I3D '99: Proceedings of the 1999 symposium on Interactive 3D graphics*. ACM, New York, NY, USA, 47–53.
- LEHNERT, H. 1993. Systematic errors of the ray-tracing algorithm. *Applied Acoustics* 38, 207–221.
- LEHTINEN, J. 2003. Time-domain numerical solution of the wave equation. [http://www.tml.tkk.fi/Opinnot/Tik-111.590/2002s/Paperit/lehtinen\\_audiosema\\_final\\_OK.pdf](http://www.tml.tkk.fi/Opinnot/Tik-111.590/2002s/Paperit/lehtinen_audiosema_final_OK.pdf).
- LEYVAND, T., SORKINE, O., AND COHEN-OR, D. 2003. Ray space factorization for from-region visibility. *ACM Transactions on Graphics* 22, 3 (July), 595–604.
- LUEBKE, D. AND GEORGES, C. 1995. Portals and mirrors: Simple, fast evaluation of potentially visible sets. *Proceedings SIGGRAPH Symposium on Interactive 3D Graphics*, 105–106.
- MEDWIN, H., CHILDS, E., AND JEBSEN, G. M. 1982. Impulse studies of double diffraction: A discrete huygens interpretation. *The Journal of the Acoustical Society of America* 72, 3, 1005–1013.
- NIRENSTEIN, S. 2003. Fast and accurate visibility preprocessing. Ph.D. thesis, University of Cape Town, South Africa.
- NIRENSTEIN, S., BLAKE, E., AND GAIN, J. 2002. Exact from-region visibility culling. In *EGRW '02: Proceedings of the 13th Eurographics workshop on Rendering*. Eurographics Association, Aire-la-Ville, Switzerland, 191–202.
- OVERBECK, R., RAMAMOORTHY, R., AND MARK, W. R. 2007. A real-time beam tracer with application to exact soft shadows. In *SR '07 Rendering Techniques*, J. Kautz and S. Pattanaik, Eds. Eurographics Association, Grenoble, France, 85–98.

- PULKKI, V., LOKKI, T., AND SAVIOJA, L. 2002. Implementation and visualization of edge diffraction with image source method. In *Proceedings of the 112th AES Convention*.
- RAGHUVANSHI, N., GALOPPO, N., AND LIN, M. C. 2008. Accelerated wave-based acoustics simulation. In *SPM '08: Proceedings of the 2008 ACM symposium on Solid and physical modeling*. ACM, New York, NY, USA, 91–102.
- SCHAUFLE, G., DORSEY, J., DECORET, X., AND SILLION, F. X. 2000. Conservative volumetric visibility with occluder fusion. In *Siggraph 2000, Computer Graphics Proceedings*, K. Akeley, Ed. Annual Conference Series. ACM Press / ACM SIGGRAPH / Addison Wesley Longman, 229–238.
- SCHRÖDER, D. AND LENTZ, T. 2006. Real-Time Processing of Image Sources Using Binary Space Partitioning. *Journal of the Audio Engineering Society (JAES)* 54, 7/8 (July), 604–619.
- SCHRÖDER, D. AND POHL, A. 2009. Real-time hybrid simulation method including edge diffraction. In *EAA Auralization Symposium*.
- SILTANEN, S., LOKKI, T., KIMINKI, S., AND SAVIOJA, L. 2007. The room acoustic rendering equation. *The Journal of the Acoustical Society of America* 122, 3 (September), 1624–1635.
- SILTANEN, S., LOKKI, T., AND SAVIOJA, L. 2009. Frequency domain acoustic radiance transfer for real-time auralization. *Acta Acustica united with Acustica* 95, 106–117(12).
- SVENSSON, P. 1999. Edge diffraction toolbox for matlab. <http://www.iet.ntnu.no/~svensson/Matlab.html>.
- SVENSSON, P. AND KRISTIANSEN, R. 2002. Computational modelling and simulation of acoustic spaces. In *22nd International Conference: Virtual, Synthetic, and Entertainment Audio*.
- SVENSSON, U. AND CALAMIA, P. 2006. Edge-diffraction impulse responses near specular-zone and shadow-zone boundaries. In *Acta Acustica united with Acustica*. Vol. 92. 501–512.
- SVENSSON, U. P., FRED, R. I., AND VANDERKOOY, J. 1999. An analytic secondary source model of edge diffraction impulse responses. *Acoustical Society of America Journal* 106, 2331–2344.
- TAYLOR, M., CHANDAK, A., REN, Z., LAUTERBACH, C., AND MANOCHA, D. 2009. Fast edge-diffraction for sound propagation in complex virtual environments. In *EAA Auralization Symposium*.
- TELLER, S. J. 1992. Computing the antipenumbra of an area light source. In *SIGGRAPH '92: Proceedings of the 19th annual conference on Computer graphics and interactive techniques*. ACM, New York, NY, USA, 139–148.
- TELLER, S. J. AND SÉQUIN, C. H. 1991. Visibility preprocessing for interactive walkthroughs. *SIGGRAPH Comput. Graph.* 25, 4, 61–70.
- TORRES, R. R., SVENSSON, U. P., AND KLEINER, M. 2001. Computation of edge diffraction for more accurate room acoustics auralization. *The Journal of the Acoustical Society of America* 109, 2, 600–610.
- TSINGOS, N., FUNKHOUSER, T., NGAN, A., AND CARLBOM, I. 2001. Modeling acoustics in virtual environments using the uniform theory of diffraction. In *Proc. of ACM SIGGRAPH*. 545–552.
- VORLANDER, M. 1989. Simulation of the transient and steady-state sound propagation in rooms using a new combined ray-tracing/image-source algorithm. *The Journal of the Acoustical Society of America* 86, 1, 172–178.
- WONKA, P., WIMMER, M., AND SCHMALSTIEG, D. 2000. Visibility preprocessing with occluder fusion for urban walkthroughs. In *Eurographics Workshop on Rendering 2000*. 71–82.
- WONKA, P., WIMMER, M., ZHOU, K., MAIERHOFER, S., HESINA, G., AND RESHETOV, A. 2006. Guided visibility sampling. In *SIGGRAPH '06: ACM SIGGRAPH 2006 Papers*. ACM, New York, NY, USA, 494–502.

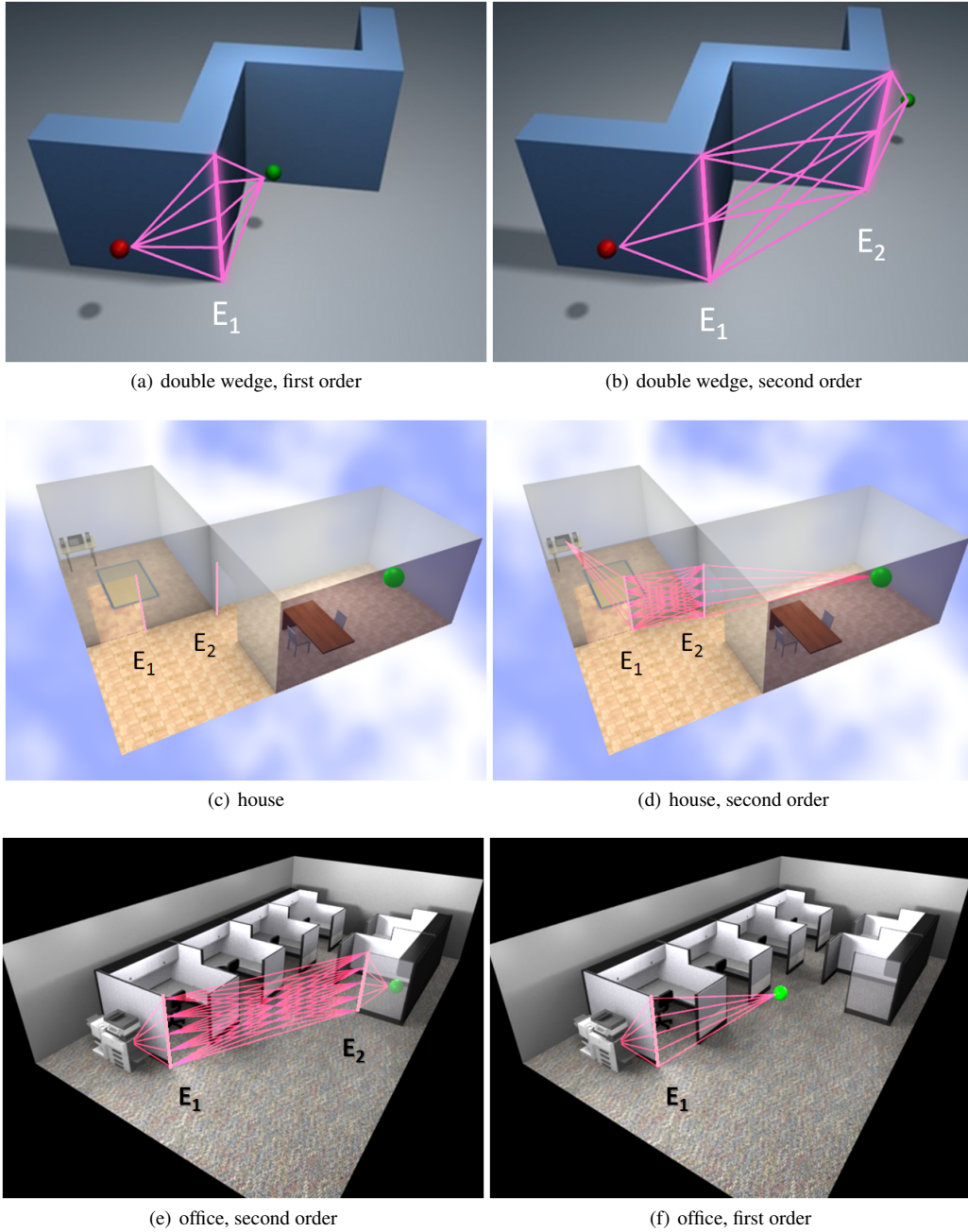


Fig. 17. Some examples of diffraction paths computed by our algorithm. Parts (a) and (b) show first and second order diffraction paths, respectively, around a wall shaped like a double wedge. Parts (c) and (d) show the House scene and a second order diffraction path in it, respectively. Parts (e) and (f) show second and first order diffraction paths, respectively, in an Office scene. In each case, diffracting edges are highlighted and labeled; for second order paths  $E_1$  is the first edge encountered along the path from source to listener, and  $E_2$  is the second edge encountered. In each case, the listener is indicated by a green sphere, and the source is indicated by a red sphere (Parts (a) and (b)), the speakers (Parts (c) and (d)) or the printer (Parts (e) and (f)). Note that in the interests of clarity, these figures show far fewer diffraction paths than are actually simulated by our algorithm.